

LIMOT: A Tightly-Coupled System for LiDAR-Inertial Odometry and Multi-Object Tracking

Zhongyang Zhu¹, Junqiao Zhao^{*,1,2}, Xuebo Tian¹, Kai Huang³, Chen Ye¹

Abstract—**Simultaneous localization and mapping (SLAM)** is critical to the implementation of autonomous driving. Most LiDAR-inertial SLAM algorithms assume a static environment, leading to unreliable localization in dynamic environments. Furthermore, accurate tracking of moving objects is of great significance for the control and planning of autonomous vehicle operation. This study proposes LIMOT, a tightly-coupled multi-object tracking and LiDAR-inertial SLAM system capable of accurately estimating the poses of both ego-vehicle and objects. First, we use 3D bounding boxes generated by an object detector to represent all movable objects and perform LiDAR odometry using inertial measurement unit (IMU) pre-integration result. Based on the historical trajectories of tracked objects in a sliding window, we perform robust object association. We propose a trajectory-based dynamic feature filtering method, which filters out features belonging to moving objects by leveraging tracking results. Factor graph-based optimization is then conducted to optimize the bias of the IMU and the poses of both the ego-vehicle and surrounding objects in a sliding window. Experiments conducted on KITTI datasets show that our method achieves better pose and tracking accuracy than our previous work DL-SLOT and other SLAM and multi-object tracking baseline methods.

I. INTRODUCTION

Simultaneous localization and mapping (SLAM) is essential for decision-making and planning of autonomous vehicles in Global Navigation Satellite System (GNSS)-denied environments. In previous studies, SLAM with only a single LiDAR or camera has been shown to achieve great success [11], [35], [6], [15]. Compared with cameras, LiDAR can directly obtain three-dimensional structural information of the environment and is largely unaffected by illumination change. However, LiDAR is unsuitable for environments that lack structural features, such as a narrow corridor; hence, many tightly-coupled LiDAR-initial SLAM systems have been proposed to improve the robustness of pose estimation [21], [16], [34], [31], [30].

Nevertheless, most SLAM systems, including LiDAR-initial SLAM, degrade in dynamic environments because

This work is supported by the National Key Research and Development Program of China (No. 2021YFB2501104). (*Corresponding Author: Junqiao Zhao*)

¹Zhongyang Zhu, Junqiao Zhao, Xuebo Tian, and Chen Ye are with Department of Computer Science and Technology, School of Electronics and Information Engineering, Tongji University, Shanghai, China, and the MOE Key Lab of Embedded System and Service Computing, Tongji University, Shanghai, China (e-mail: 2233057@tongji.edu.cn; zhaojunqiao@tongji.edu.cn; 1930773@tongji.edu.cn; yechen@tongji.edu.cn).

²Institute of Intelligent Vehicles, Tongji University, Shanghai, China

³Kai Huang is with the School of Surveying and Geo-Informatics, Tongji University, Shanghai, China (e-mail: 1911202@tongji.edu.cn).

they rely heavily on the assumption of a static environment. Therefore, it is crucial for SLAM to use reasonable approaches to deal with dynamic objects in real-world applications. At the same time, multi-object tracking in complex dynamic scenes is crucial for the decision-making and planning of autonomous vehicles. The combination of SLAM and multi-object tracking has become an important task and has been widely studied in recent years. The vast majority of methods perform MOT and SLAM separately, i.e., loosely-coupled. This results in that the tracking accuracy highly depends on ego-pose estimation, which is, however, not reliable in dynamic environments.

Recently, tightly-coupled multi-object tracking and vision-based SLAM systems have gained extensive attention. These systems generally construct a unified optimization framework, in which the poses of both the ego-vehicle and moving objects are jointly optimized. However, their performance is nonetheless limited by inaccurate 3D object detection and sensitivity to illumination change and rapid motion.

In a previous study, we developed DL-SLOT [24], a tightly-coupled LiDAR SLAM and multi-object tracking system; although effective, it is still subject to the limitations of the single LiDAR sensor described above. Therefore, it is necessary to develop the tight coupling of multi-object tracking and LiDAR-inertial SLAM. In this paper, we propose LIMOT, a tightly-coupled multi-object tracking and LiDAR-inertial SLAM system capable of accurately estimating the poses of both the ego-vehicle and surrounding objects. First, all movable objects are represented by 3D bounding boxes generated by an object detector. Simultaneously, the estimated motion from inertial measurement unit (IMU) pre-integration de-skews LiDAR scans and provides an initial guess for scan-matching, thereby obtaining the LiDAR odometry. Then, similar to DL-SLOT, a combination of trajectory approximation of tracked objects in a sliding window and the continuous shortest path algorithm [1] is employed to perform data association. Object states (stationary or dynamic) can be obtained through tracking results. Based on the constant velocity model and the estimated motion from IMU pre-integration, the poses of moving objects in the world frame can be predicted. Therefore, feature points belonging to moving objects can be precisely filtered out based on the approximated object trajectories before scan-matching; as such, scan-matching is unaffected by dynamic feature points. Finally, a factor graph optimization framework is conducted to optimize the bias of the IMU and the poses of both the ego-vehicle and objects in a sliding window. The main contributions of this work can be summarized as

follows:

- Development of a tightly-coupled multi-object tracking and LiDAR-initial SLAM system, allowing for joint estimation of the poses of both the ego-vehicle and surrounding objects.
- Introduction of a method that leverages the approximated object trajectories to identify and exclude feature points belonging to moving objects, while still utilizing feature points on static objects to provide constraints for scan-matching.

II. RELATED WORKS

A. LiDAR-initial SLAM

Schemes relating to the fusion of LiDAR and IMU measurements can be classified into two categories: loosely-coupled fusion [35], [20], [13], [7], [32] and tightly-coupled fusion [21], [16], [34], [31], [30]. In LOAM [35] and LeGO-LOAM [20], IMU measurements are used to de-skew LiDAR scans and provide a motion prior to scan registration. In [13], [7], [32], the extended Kalman filter is employed to loosely fuse LiDAR, IMU, and optionally GNSS for robot pose estimation. However, the IMU bias is not optimized in these loosely-coupled algorithms, thereby reducing their precision. LINS [16] proposed a tightly-coupled LiDAR-inertial odometry method based on an iterated Kalman filter. Similar to [16], FAST-LIO [31] also utilizes the iterated Kalman filter but introduces a new Kalman gain to reduce the complexity of computation. Based on [31], FAST-LIO2 [30] directly registers raw points without extracting features and introduces the iKD-Tree to increase mapping rate and odometry accuracy. LIOM [34] jointly optimizes LiDAR-IMU extrinsic parameters, IMU bias, and robot pose using graph-based optimization. It achieves better accuracy when compared with LOAM; however, the algorithm suffers from computational inefficiency. LIO-SAM [21] estimates IMU bias in the factor graph exhibiting better real-time performance than LIOM and achieving accurate and robust state estimation. However, all of these LiDAR-initial methods depend on the assumption of the static environment and are easily disturbed by moving objects.

B. Dynamic SLAM and Multi-object Tracking

During the past decade, researchers have increasingly focused on the study of SLAM for dynamic environments. The traditional dynamic SLAM approaches mainly reject information from all movable objects to ensure the robustness of the system, which reduces the information available for SLAM and thus degrades the SLAM performance [4], [25], [5], [37].

In recent years, the SLAM and multi-object tracking system in dynamic environments has been increasingly investigated and can be classified into loosely and tightly-coupled approaches. In the former, SLAM and multi-object tracking are performed independently [26], [14], [19]. SLAMMOT[26] first proposed simultaneously estimating ego-motion and multi-object motion, establishing a mathematical framework to decompose the estimation problem into

two separated filter-based estimators. MaskFusion [19], an RGB-D SLAM system, uses both photometric and geometric information to track the detected objects in the scene. [14] estimates ego-motion based on the static background and achieves object tracking through the least-squares method by fusing point clouds and 3D detection. However, the accuracy of multi-object tracking in these methods is heavily dependent on ego-pose estimation, which likely fails in complex dynamic environments.

Tightly-coupled multi-object tracking and SLAM methods are primarily proposed in visual SLAM systems [33], [36], [3], [9]. Specifically, CubeSLAM [33] firstly proposed the use of a multi-view bundle adjustment (BA) to jointly optimize ego-pose, states of objects, and feature points using only a monocular camera. Dynamic objects are tracked by a 2D visual object tracking algorithm [10]. VDO-SLAM [36] tracks feature points on objects by leveraging dense optical flow. Motion model constraints are added to the factor graph to effectively enable the combined optimization of ego-pose and object states. DynaSLAM II [3] makes use of instance semantic segmentation and ORB feature [18] correspondences to track moving objects, jointly optimizing the static structure and trajectories of the camera and moving objects in a local-temporal window. [9] achieves data association using optical flow estimation and performs a novel joint optimization BA by defining inter-cluster constraints modeled by mechanical joints. These vision-based methods mostly perform tracking in 2D image space and thus suffer from inaccurate 3D object detection, textureless or low-illumination environments, and greater susceptibility to occlusion.

Among LiDAR-based methods, our previous work DL-SLOT[24] was, to the best of our knowledge, the first tightly-coupled LiDAR SLAM and multi-object tracking system. However, it is also subject to LiDAR degradation scenes. The experiments shown in this paper indicate that the present method substantially outperforms DL-SLOT in terms of pose accuracy.

A recent approach, LIO-SEGMOT [12], proposed an optimization framework similar to ours, but without a sliding window. As a result, it is computationally expensive when there are multiple objects for tightly-coupled optimization and the cost increases with an increasing number of objects. In addition, this method does not remove dynamic points, thus exhibiting almost no improvement in pose accuracy on the public dataset compared to LIO-SAM. In contrast, the system described herein achieves more accurate localization and limits the cost of joint optimization of the poses of the ego-vehicle and objects through a sliding window.

III. METHODS

A. System Overview

We here define the frames and main notations used throughout this paper. We consider W as the world frame and I_k , L_k as the IMU and LiDAR frames, related to the k -th LiDAR scan at time t_k , respectively. We denote $\mathbf{T}_b^a \in SE(3)$ as the pose of frame b in a . $\mathbf{R}_b^a \in SO(3)$ and

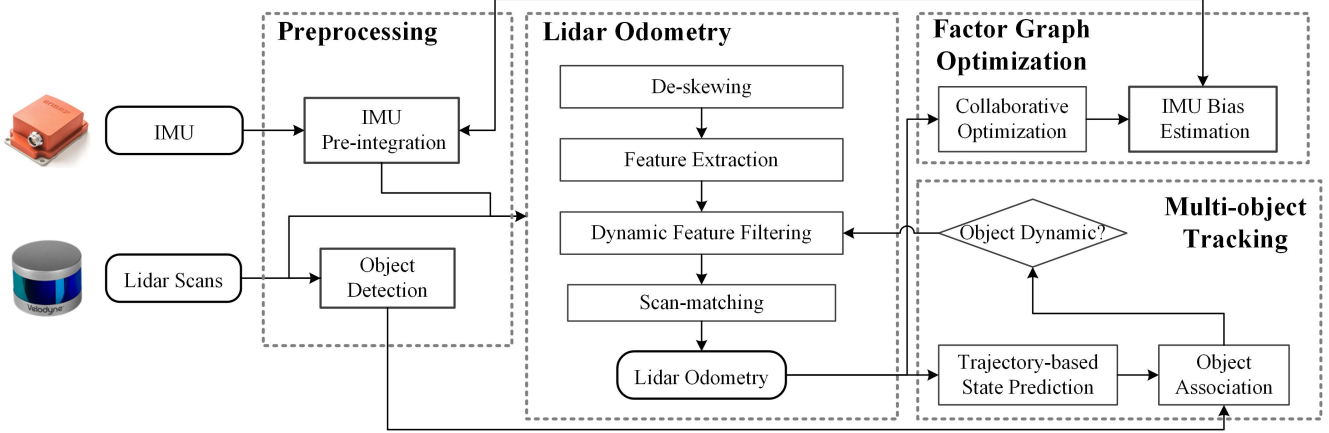


Fig. 1. The system architecture of LIMOT. The system consists of the preprocessing, LiDAR odometry, the sliding window-based 3D multi-object tracking, and factor graph optimization.

$\mathbf{p}_b^a \in \mathbb{R}^3$ are the rotation matrix and translation vector of \mathbf{T}_b^a , respectively. The quaternion \mathbf{q}_b^a under Hamilton notation is used, corresponding to \mathbf{R}_b^a . \mathbf{g}^W is the gravity vector in frame W . We also assume that the LiDAR frame coincides with the ego-vehicle frame for convenience. Therefore, the pose of the ego-vehicle in frame W at t_k is represented as $\mathbf{T}_{L_k}^W$ and the pose transformation from t_{k-1} to t_k is represented as $\mathbf{T}_{L_k}^{L_{k-1}}$. For simplification, we denote $\mathbf{T}_{L_k}^W$ as \mathbf{T}_k^W and $\mathbf{T}_{L_k}^{L_{k-1}}$ as $\mathbf{T}_k^{L_{k-1}}$. In addition, the j -th object in W and the ego-vehicle frame at t_k are represented as \mathbf{T}_{k,O_j}^W and \mathbf{T}_{k,O_j}^L , respectively. Each can be converted into the other as follows:

$$\mathbf{T}_{k,O_j}^W = \mathbf{T}_k^W \cdot \mathbf{T}_{k,O_j}^L \quad (1)$$

We choose LIO-SAM as our baseline method since its optimization process is based on the factor graph framework, which is relatively easy to extend [22], [29]. An overview of the proposed system is shown in Figure 1. During preprocessing (Section III-B), we use 3D bounding boxes generated by an object detector to represent all movable objects and perform IMU pre-integration. The predicted ego-pose from IMU pre-integration can de-skew point clouds and provide an initial guess for scan-matching (Section III-D). Prior to scan-matching, a trajectory-based dynamic feature filtering method is performed to filter out features belonging to moving objects by leveraging tracking results and the predicted ego-pose. 3D multi-object tracking (Section III-C) is then performed between the tracked and detected objects using trajectories within a sliding window. Finally, a factor graph optimization framework (Section III-E) is utilized to optimize the bias of the IMU and the poses of both ego-vehicle and objects in a sliding window.

B. Preprocessing

1) *Object Detection*: To simplify the object observation model, we use open source 3D LiDAR object detectors, such as PointRCNN [23], to generate the 3D bounding box and pose in LiDAR frame \mathbf{T}_{k,O_j}^L of an object.

2) *IMU Pre-integration*: We perform IMU pre-integration to aggregate raw IMU measurements in the local frame, following [17]. IMU measurements contain linear acceleration $\hat{\mathbf{a}}$ and angular velocity $\hat{\boldsymbol{\omega}}$ affected by acceleration bias \mathbf{b}_a and gyroscope bias \mathbf{b}_w . Given the bias estimation, IMU measurements in time interval $[t_k, t_{k+1}]$ can be integrated in local frame I_k as follows:

$$\begin{aligned} \boldsymbol{\alpha}_{I_{k+1}}^{I_k} &= \iint_{t \in [t_k, t_{k+1}]} \mathbf{R}_{I_t}^{I_k} (\hat{\mathbf{a}}_t - \mathbf{b}_{a_t}) dt^2 \\ \boldsymbol{\beta}_{I_{k+1}}^{I_k} &= \int_{t \in [t_k, t_{k+1}]} \mathbf{R}_{I_t}^{I_k} (\hat{\mathbf{a}}_t - \mathbf{b}_{a_t}) dt \\ \boldsymbol{\gamma}_{I_{k+1}}^{I_k} &= \int_{t \in [t_k, t_{k+1}]} \frac{1}{2} \boldsymbol{\Omega} (\hat{\boldsymbol{\omega}}_t - \mathbf{b}_{w_t}) \boldsymbol{\gamma}_{I_t}^{I_k} dt \end{aligned} \quad (2)$$

with

$$\boldsymbol{\Omega}(\boldsymbol{\omega}) = \begin{bmatrix} -[\boldsymbol{\omega}]_\times & \boldsymbol{\omega} \\ -\boldsymbol{\omega}^T & 0 \end{bmatrix}, [\boldsymbol{\omega}]_\times = \begin{bmatrix} 0 & -\omega_z & \omega_y \\ \omega_z & 0 & -\omega_x \\ -\omega_y & \omega_x & 0 \end{bmatrix}$$

where $\boldsymbol{\alpha}_{I_{k+1}}^{I_k}$, $\boldsymbol{\beta}_{I_{k+1}}^{I_k}$, and $\boldsymbol{\gamma}_{I_{k+1}}^{I_k}$ represent the relative position, velocity, and rotation of the IMU frame within two consecutive frames I_k and I_{k+1} . It can be seen that the pre-integration terms can be computed solely using IMU measurements and are independent of the initial state in frame I_k .

C. Multi-object Tracking

We use an approach similar to DL-SLOT to predict the position of the tracked object by fitting its trajectory in a sliding window with a cubic order polynomial. Then, a matching matrix is generated by calculating the distances between the detected objects in the current scan and the predicted positions of the tracked objects in the previous scan. The continuous shortest path algorithm [1] is employed to perform data association based on the matching matrix.

After completing object association, the average velocities of the objects within the sliding window are calculated. An object is determined to be dynamic, then its average velocity is greater than a given threshold.

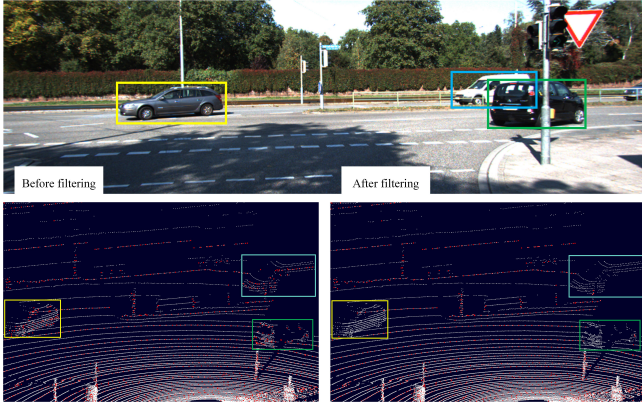


Fig. 2. Example result of filtering out dynamic feature points. The white points denote the original point cloud and the red points denote the feature points. The feature points on the dynamic vehicles (shown in the image) are removed exactly.

D. LiDAR Odometry

1) De-skewing, Feature Extraction and Scan-matching:

For point cloud de-skewing, a nonlinear motion model is utilized with the estimated motion from the IMU, which is more precise than using a linear motion model [34]. Edge and planar feature points are then extracted based on the local roughness of the point cloud. After removing feature points belonging to moving objects (see Section III-D.2), point-to-edge and point-to-plane scan-matching is conducted between the current scan at t_k and the submap composed of a fixed-size set of history scans to obtain ego-pose \mathbf{T}_k^W . The initial transformation guess is obtained using the predicted ego-motion, $\tilde{\mathbf{T}}_k^W$, from IMU pre-integration.

2) Trajectory-based Dynamic Feature Filtering: For dynamic objects at t_k , we use their fitted trajectories generated by the multi-object tracking module to predict their positions at t_{k+1} . Based on the predicted ego-pose $\tilde{\mathbf{T}}_{k+1}^W$ at t_{k+1} , feature points located within the 3D bounding boxes of dynamic objects can be filtered out from the $k+1$ -th point cloud before scan-matching. An example result is shown in Figure 2.

E. Joint Factor Graph Optimization

The joint factor graph optimization framework is shown in Figure 3. It consists of the factors providing constraints for optimization and variable nodes including the states of the ego-vehicle and surrounding objects. We add only one object pose node to the factor graph when the object is judged as stationary to ensure the uniqueness of the global pose of the stationary object, which can provide reliable static observation constraints. The residual formulation corresponding to each factor in Figure 3 is given below.

The residual of the IMU pre-integration factor related to ego-states and pre-integrated IMU measurements

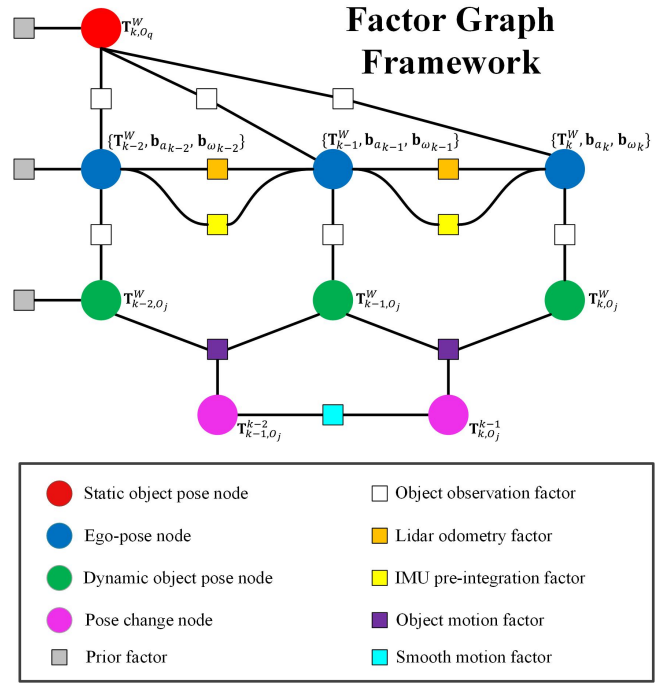


Fig. 3. Factor graph framework of LIMOT for joint optimization.

$[\hat{\alpha}_{I_{k+1}}^{I_k}, \hat{\beta}_{I_{k+1}}^{I_k}, \hat{\gamma}_{I_{k+1}}^{I_k}]$ can be defined as:

$$\begin{aligned}
 \mathbf{r}_I^k(\mathcal{X}) &= \begin{bmatrix} \delta\alpha_{I_{k+1}}^{I_k} \\ \delta\beta_{I_{k+1}}^{I_k} \\ \delta\theta_{I_{k+1}}^{I_k} \\ \delta\mathbf{b}_a \\ \delta\mathbf{b}_g \end{bmatrix} \\
 &= \begin{bmatrix} \mathbf{R}_W^{I_k} \left(\mathbf{p}_{I_{k+1}}^W - \mathbf{p}_{I_k}^W + \frac{1}{2}\mathbf{g}^W \Delta t_k^2 - \mathbf{v}_{I_k}^W \Delta t_k \right) - \hat{\alpha}_{I_{k+1}}^{I_k} \\ \mathbf{R}_W^{I_k} \left(\mathbf{v}_{I_{k+1}}^W + \mathbf{g}^W \Delta t_k - \mathbf{v}_{I_k}^W \right) - \hat{\beta}_{I_{k+1}}^{I_k} \\ 2 \left[\mathbf{q}_{I_k}^{W^{-1}} \otimes \mathbf{q}_{I_{k+1}}^W \otimes \left(\hat{\gamma}_{I_{k+1}}^{I_k} \right)^{-1} \right]_{xyz} \\ \mathbf{b}_{a_{k+1}} - \mathbf{b}_{a_k} \\ \mathbf{b}_{w_{k+1}} - \mathbf{b}_{w_k} \end{bmatrix} \quad (3)
 \end{aligned}$$

where $\delta\theta_{I_{k+1}}^{I_k}$ represents the three-dimensional relative rotation error in Euclidean space and $[\cdot]_{xyz}$ represents the vector part of quaternion \mathbf{q} .

Given the ego-poses at t_{k-1} and t_k estimated by LiDAR scan-matching, the residual of the LiDAR odometry factor can be defined as follows:

$$\mathbf{r}_{odo}^k(\mathbf{T}_{k-1}^W, \mathbf{T}_k^W) = (\mathbf{T}_{k-1}^{W^{-1}} \cdot \mathbf{T}_k^W) \cdot \mathbf{T}_k^{k-1-1} \quad (4)$$

Then, based on the object detection results, the residual of the object observation factor is defined as follows:

$$\mathbf{r}_{obs}^{k,j}(\mathbf{T}_k^W, \mathbf{T}_{k,O_j}^W) = (\mathbf{T}_k^{W^{-1}} \cdot \mathbf{T}_{k,O_j}^W) \cdot \mathbf{T}_{k,O_j}^{L-1} \quad (5)$$

The pose change of object \mathbf{T}_{k,O_j}^{k-1} between t_{k-1} and t_k can be calculated using Equation 6, which also indicates the velocity of the object. The object motion factor is a ternary factor associated with three nodes: two dynamic object pose

TABLE I

THE TRANSLATION RMSE(M) AND ROTATION RMSE(RAD) RESULTS OF EGO-POSE ESTIMATION COMPARISON ON THE KITTI TRACKING DATASET

Seq	LIO-SAM		LIO-filter(Ours)		DL-SLOT		LIMOT(Ours)	
	RMSE(m)	RMSE(rad)	RMSE(m)	RMSE(rad)	RMSE(m)	RMSE(rad)	RMSE(m)	RMSE(rad)
04	0.660	0.104	0.571	0.085	1.151	0.257	0.539	0.086
07	1.317	0.025	1.329	0.023	1.002	0.274	1.504	0.027
08	1.269	0.306	1.141	0.268	1.765	0.319	1.131	0.268
09	1.195	0.024	1.208	0.024	3.548	1.121	1.321	0.022
11	0.262	0.198	0.257	0.200	0.218	0.266	0.265	0.026
15	0.275	0.066	0.276	0.066	0.300	0.374	0.268	0.068
18	0.385	0.141	0.368	0.160	0.676	0.172	0.367	0.160
19	1.858	0.049	1.789	0.048	1.552	0.564	1.436	0.048
20	9.488	0.021	4.934	0.023	11.694	0.040	4.219	0.023
mean	1.857	0.104	1.319	0.100	2.434	0.376	1.228	0.081

TABLE II

THE TRANSLATION RMSE(M) AND ROTATION RMSE(RAD) RESULTS OF EGO-POSE ESTIMATION COMPARISON ON THE KITTI ODOMETRY DATASET

Seq	LIO-SAM		LIO-filter		DL-SLOT		LIMOT	
	RMSE(m)	RMSE(rad)	RMSE(m)	RMSE(rad)	RMSE(m)	RMSE(rad)	RMSE(m)	RMSE(rad)
05	4.312	0.030	3.986	0.036	7.012	0.530	4.121	0.036
07	0.828	0.019	0.654	0.012	2.620	0.776	0.547	0.015
08	5.073	0.037	5.138	0.037	10.829	0.609	5.005	0.038
09	3.894	0.048	3.929	0.030	5.685	0.658	3.941	0.025
mean	3.527	0.034	3.427	0.029	6.537	0.643	3.404	0.029

nodes \mathbf{T}_{k-1,O_j}^W , \mathbf{T}_{k,O_j}^W and one pose change node \mathbf{T}_{k,O_j}^{k-1} . These are continually updated throughout the optimization process, but the relationship between them should always satisfy Equation 6. Thus, the residual of the object motion factor is defined by Equation 7.

$$\mathbf{T}_{k,O_j}^{k-1} = \mathbf{T}_{k-1,O_j}^W \cdot \mathbf{T}_{k,O_j}^W^{-1} \cdot \mathbf{T}_{k,O_j}^W \quad (6)$$

$$\mathbf{r}_{moti}^k(\mathbf{T}_{k-1,O_j}^W, \mathbf{T}_{k,O_j}^W, \mathbf{T}_{k,O_j}^{k-1}) = (\mathbf{T}_{k-1,O_j}^W \cdot \mathbf{T}_{k,O_j}^W) \cdot \mathbf{T}_{k,O_j}^{k-1} \quad (7)$$

We further assume that a dynamic object moves at a constant velocity over a short period of time, such the pose changes of the object at successive times should be almost identical. Therefore, the residual of the smooth motion factor is defined as follows:

$$\mathbf{r}_{smoo}^k(\mathbf{T}_{k-1,O_j}^{k-2}, \mathbf{T}_{k,O_j}^{k-1}) = \mathbf{T}_{k-1,O_j}^{k-2} \cdot \mathbf{T}_{k,O_j}^{k-1} \quad (8)$$

Finally, the optimization problem can be denoted as:

$$\begin{aligned} \mathcal{X}^* = \arg\min_{\mathcal{X}} \Big\{ & \|\mathbf{r}_P(\mathcal{X})\|^2 + \sum_{k \in \mathcal{I}} \|\mathbf{r}_I^k(\mathcal{X})\|_{Q_I}^2 \\ & + \sum_{k \in \mathcal{L}} \left(\|\mathbf{r}_{odo}^k(\mathcal{X})\|_{Q_{odo}}^2 + \sum_{j \in \mathcal{O}_k} \left(\|\mathbf{r}_{obs}^{k,j}(\mathcal{X})\|_{Q_{obs}}^2 \right. \right. \\ & \left. \left. + \|\mathbf{r}_{moti}^{k,j}(\mathcal{X})\|_{Q_{moti}}^2 + \|\mathbf{r}_{smoo}^{k,j}(\mathcal{X})\|_{Q_{smoo}}^2 \right) \right) \Big\} \quad (9) \end{aligned}$$

where \mathcal{X} is the set of all variables, $\|\mathbf{r}_P(\mathcal{X})\|^2$ is the prior items from marginalization, \mathcal{I} is the set of all IMU measurements, \mathcal{L} is the set of LiDAR scans in the sliding window, and Q represents the covariance matrix. Each LiDAR scan is related to the tracked object set \mathcal{O}_k . For practical implementation, the states of the ego-vehicle and the objects are first jointly optimized without considering the residuals

of the IMU pre-integration factor. Subsequently, the IMU bias is estimated based on the optimized ego-vehicle poses. This process ensures the robustness and efficiency of the optimization.

IV. EXPERIMENTS

We conducted experiments using the public dataset KITTI [8] to evaluate the performance of the proposed LIMOT. The experiments are divided into two parts, one to evaluate the accuracy of the ego-pose, and another to evaluate the performance of multi-object tracking. To reduce the impact of inaccurate detection due to sparse scanning, objects located within 3 to 45 m in front of the ego-vehicle are considered. Experiments were carried out on a PC with Ubuntu 20.04, equipped with an Intel Core Xeon(R) Gold 6248R 3.00GHz processor and 32G RAM.

A. Ego-pose Evaluation

We used the KITTI Tracking and Odometry datasets for ego-pose evaluation. These datasets were collected in urban areas and along highways and contain raw point clouds, as well as GNSS/IMU data. The root-mean-square error (RMSE) of the absolute trajectory error (ATE) is adopted to assess the accuracy of ego-poses. The baseline methods are DL-SLOT [24] and LIO-SAM [21]. LIO-SAM is one of the state-of-the-art (SOTA) LiDAR-inertial SLAM methods, on which we build LIMOT. When only dynamic feature point removal is performed without jointly optimizing the poses of the ego-vehicle and objects, our method is referred to as LIO-filt. We chose the same sequences as DL-SLOT.

The comparative results on the KITTI Tracking dataset are shown in Table I. The pose accuracy of LIO-filt is higher than

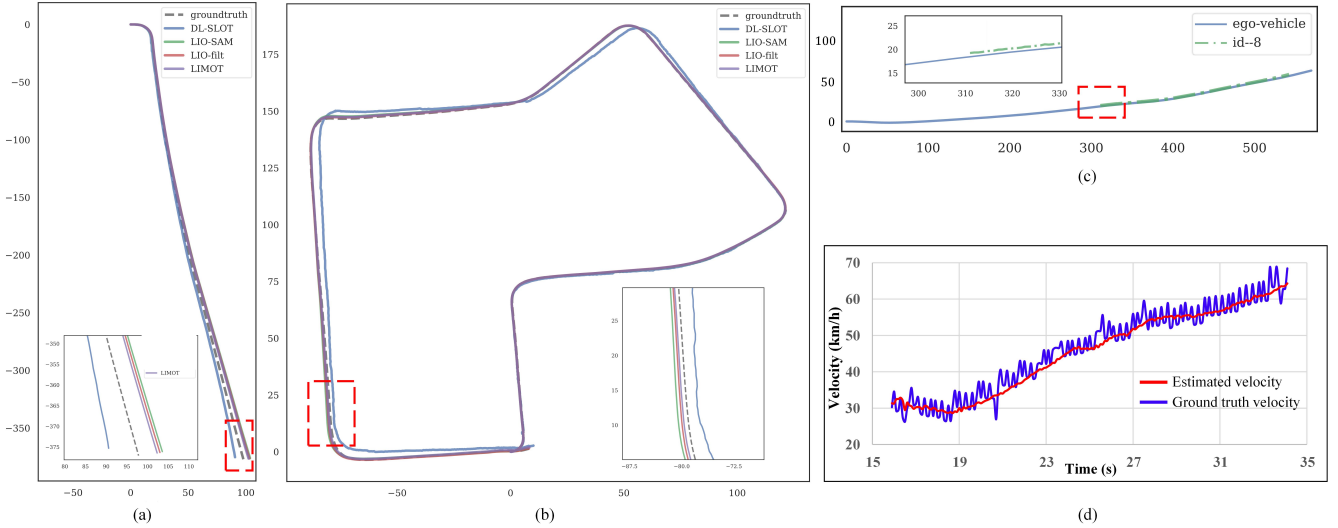


Fig. 4. Qualitative results of LIMOT on the KITTI dataset. (a) Comparison of ego-trajectories in sequence 04 of the KITTI Tracking dataset. (b) Comparison of ego-trajectories in sequence 07 of the KITTI Odometry dataset. (c) Trajectories of the main tracked object (id 8) and ego-vehicle in sequence 08 of the KITTI Tracking dataset. (d) Comparison between the ground truth and estimated instantaneous velocity of the tracked object in (c).

that of LIO-SAM, demonstrating the effectiveness of our proposed trajectory-based dynamic feature filtering approach. Compared to DL-SLOT, methods tightly coupled with IMU, i.e., LIO-SAM and LIMOT, both achieved better performance, demonstrating that coupling IMU assists in localization. LIMOT achieved the best pose estimation performance, confirming that jointly optimizing the poses of the ego-vehicle and objects is beneficial. It is particularly important to note that sequence 20 is a highway scene containing a large number of moving objects. Since the highway is a typical scene for LiDAR SLAM degradation, DL-SLOT shows a large translation error and both LIMOT and LIO-filter have a large improvement compared to LIO-SAM.

The KITTI Odometry dataset provides complex long odometry tasks. As shown in Table II, LIMOT outperforms the other methods on average.

The ego-trajectory comparisons of sequence 04 on the KITTI Tracking dataset and sequence 07 on the KITTI Odometry dataset are demonstrated in Figure 4 (a) and (b), respectively.

B. Multi-object Tracking Performance Evaluation

The performance of multi-object tracking is evaluated in two ways. The multi-object tracking accuracy (MOTA) metric [2] is used to evaluate tracking accuracy. Then, we evaluated the pose accuracy of the objects, using the RMSE of ATE.

1) *Tracking Accuracy Evaluation*: We selected two popular LiDAR-based 3D multi-object tracking methods, AB3DMOT [27] and PC3T [28], as well as our previous work DL-SLOT for comparison. AB3DMOT first proposed to directly evaluate MOTA in 3D space, which is more suitable for LiDAR-based approaches. PC3T is a published SOTA method requiring ground truth ego-poses as input. Each of these methods uses the same object detector PointR-

CNN [23]. The comparison results are shown in Table III. For each tracked object, its Intersection over Union (IoU) with ground truth label should exceed a threshold IoU_{thres} to be considered as a successful match. It can be found that our method shows the best results in terms of MOTA on average. Specifically, it achieves more significant improvement when evaluated with a higher IoU_{thres} , indicating that our method obtains more accurate object poses.

TABLE III
MOTA RESULTS COMPARISON OF DIFFERENT MULTI-OBJECT
TRACKING ALGORITHMS ON THE KITTI TRACKING DATASET

Matching criteria	AB3DMOT	PC3T	DL-SLOT	LIMOT
$\text{IoU}_{thres} = 0.25$	0.8556	0.8735	0.8610	0.8648
$\text{IoU}_{thres} = 0.5$	0.8341	0.8592	0.8514	0.8617
$\text{IoU}_{thres} = 0.7$	0.6231	0.7210	0.6740	0.7633
mean	0.7709	0.8179	0.7955	0.8299

2) *Object Pose Evaluation*: We further evaluated the pose accuracy of the objects as well as their tracking frame length (TFL). We selected the object with the longest TFL in each sequence for evaluation. The experimental results are shown in Table IV. Since we use a similar tracking method as DL-SLOT, the TFL results of these two methods are the same. However, the pose accuracy of the objects is improved significantly, largely due to the reduction of the ego-pose rotation error of LIMOT by virtue of coupling IMU measurements.

The trajectories of the tracked object (id 8) and ego-vehicle in sequence 08 are demonstrated in Figure 4 (c). The blue solid line and the green dotted line represent the trajectories of the ego-vehicle and the tracked object, respectively.

We further compare the estimated instantaneous velocity of the object (id 8) in sequence 08 with the ground truth. As shown in Figure 4 (d), the ground truth instantaneous

velocities (blue line) exhibit significant fluctuation due to the error in object annotations within the dataset. In contrast, the estimated instantaneous velocities (red line) are smoother and in the middle of the fluctuation range of the ground truth. This indicates that it is appropriate to add the constant velocity constraint to the factor graph optimization.

TABLE IV
RESULTS OF OBJECT POSE ESTIMATION COMPARISON ON THE KITTI
TRACKING DATASET

Seq / id	TFL	DL-SLOT		LIMOT	
		RMSE(m)	RMSE(rad)	RMSE(m)	RMSE(rad)
04 / 2	88	1.311	0.224	0.211	0.028
07 / 55	45	1.111	0.407	0.171	0.063
08 / 8	184	0.468	0.054	0.388	0.067
09 / 9	30	0.332	0.048	0.118	0.040
11 / 0	372	0.321	0.062	0.316	0.116
15 / 18	169	0.212	0.039	0.192	0.084
18 / 3	257	0.384	0.550	0.375	0.480
19 / 63	131	0.484	0.317	0.343	0.228
20 / 12	603	3.646	0.034	0.905	0.023
mean		0.919	0.193	0.335	0.125

C. Running Time Analysis

We calculated the average time-consumption of the main functional modules except for object detection. As shown in Table V, the method proposed in this study is able to achieve real-time performance. Compared with LIO-SAM, the time consumption of LiDAR odometry and factor graph optimization increase by 0.2 ms and 6.3 ms, respectively, which correspond to the runtime of the dynamic feature filtering and joint optimization of the states of objects.

TABLE V
AVERAGE TIME-CONSUMING OF THE MAIN FUNCTIONAL MODULES
FOR PROCESSING ONE SCAN

Module	Average Runtime (ms)
LiDAR Odometry	69.2 + 0.2
Multi-object Tracking	7.1
Factor Graph Optimization	1.5 + 6.3

V. CONCLUSIONS

We present LIMOT, a tightly-coupled system for LiDAR-inertial SLAM and multi-object tracking capable of jointly optimizing the poses of the ego-vehicle and surrounding objects in a sliding window. Furthermore, this method can filter out feature points belonging to moving objects based on the approximated object trajectories, while the remaining feature points on static objects are used to provide constraints for scan-matching, which enhances the robustness of the system and improves its performance in dynamic environments. Experimental results show that our method improves the pose accuracy of ego-vehicle and objects, as well as the tracking accuracy, which demonstrates that LiDAR-inertial SLAM and multi-object tracking can exhibit mutual benefits on each other.

In the future, it will be advantageous to introduce a dynamics model for moving objects in the environment to obtain more accurate object poses. Future work could also involve the utilization of visual data to assist object detection and LiDAR-inertial SLAM.

REFERENCES

- [1] Ravindra K Ahuja, Thomas L Magnanti, and James B Orlin. Network flows. 1988.
- [2] Keni Bernardin and Rainer Stiefelhagen. Evaluating multiple object tracking performance: the clear mot metrics. *EURASIP Journal on Image and Video Processing*, 2008:1–10, 2008.
- [3] Berta Bescos, Carlos Campos, Juan D. Tardós, and José Neira. Dynaslam ii: Tightly-coupled multi-object tracking and slam. *IEEE Robotics and Automation Letters*, 6(3):5191–5198, 2021.
- [4] Berta Bescos, José M Fácil, Javier Civera, and José Neira. Dynaslam: Tracking, mapping, and inpainting in dynamic scenes. *IEEE Robotics and Automation Letters*, 3(4):4076–4083, 2018.
- [5] Xieyuanli Chen, Andres Milioto, Emanuele Palazzolo, Philippe Giguere, Jens Behley, and Cyrill Stachniss. Suma++: Efficient lidar-based semantic slam. In *2019 IEEE/RSJ International Conference on Intelligent Robots and Systems (IROS)*, pages 4530–4537. IEEE, 2019.
- [6] Andrew J Davison, Ian D Reid, Nicholas D Molton, and Olivier Stasse. Monoslam: Real-time single camera slam. *IEEE transactions on pattern analysis and machine intelligence*, 29(6):1052–1067, 2007.
- [7] Mahmut Demir and Kikuo Fujimura. Robust localization with low-mounted multiple lidars in urban environments. In *2019 IEEE Intelligent Transportation Systems Conference (ITSC)*, pages 3288–3293. IEEE, 2019.
- [8] Andreas Geiger, Philip Lenz, and Raquel Urtasun. Are we ready for autonomous driving? the kitti vision benchmark suite. In *Conference on Computer Vision and Pattern Recognition (CVPR)*, 2012.
- [9] Mathieu Gonzalez, Eric Marchand, Amine Kacete, and Jerome Royan. Twistslam: Constrained slam in dynamic environment. *IEEE Robotics and Automation Letters*, 7(3):6846–6853, 2022.
- [10] João F Henriques, Rui Caseiro, Pedro Martins, and Jorge Batista. High-speed tracking with kernelized correlation filters. *IEEE transactions on pattern analysis and machine intelligence*, 37(3):583–596, 2014.
- [11] Wolfgang Hess, Damon Kohler, Holger Rapp, and Daniel Andor. Real-time loop closure in 2d lidar slam. In *2016 IEEE international conference on robotics and automation (ICRA)*, pages 1271–1278. IEEE, 2016.
- [12] Yu-Kai Lin, Wen-Chieh Lin, and Chieh-Chih Wang. Asynchronous state estimation of simultaneous ego-motion estimation and multiple object tracking for lidar-inertial odometry. pages 1–7, 2023.
- [13] Simon Lynen, Markus W Achtelik, Stephan Weiss, Margarita Chli, and Roland Siegwart. A robust and modular multi-sensor fusion approach applied to mav navigation. In *2013 IEEE/RSJ international conference on intelligent robots and systems*, pages 3923–3929. IEEE, 2013.
- [14] Tingchen Ma and Yongsheng Ou. Mlo: Multi-object tracking and lidar odometry in dynamic environment. *arXiv preprint arXiv:2204.11621*, 2022.
- [15] Raul Mur-Artal, Jose Maria Martinez Montiel, and Juan D Tardos. Orb-slam: a versatile and accurate monocular slam system. *IEEE transactions on robotics*, 31(5):1147–1163, 2015.
- [16] Chao Qin, Haoyang Ye, Christian E Pranata, Jun Han, Shuyang Zhang, and Ming Liu. Lins: A lidar-inertial state estimator for robust and efficient navigation. In *2020 IEEE international conference on robotics and automation (ICRA)*, pages 8899–8906. IEEE, 2020.
- [17] Tong Qin, Peiliang Li, and Shaojie Shen. Vins-mono: A robust and versatile monocular visual-inertial state estimator. *IEEE Transactions on Robotics*, 34(4):1004–1020, 2018.
- [18] Ethan Rublee, Vincent Rabaud, Kurt Konolige, and Gary Bradski. Orb: An efficient alternative to sift or surf. In *2011 International conference on computer vision*, pages 2564–2571. Ieee, 2011.
- [19] Martin Runz, Maud Buffier, and Lourdes Agapito. Maskfusion: Real-time recognition, tracking and reconstruction of multiple moving objects. In *2018 IEEE International Symposium on Mixed and Augmented Reality (ISMAR)*, pages 10–20. IEEE, 2018.
- [20] Tixiao Shan and Brendan Englot. Lego-loam: Lightweight and ground-optimized lidar odometry and mapping on variable terrain. In *IEEE/RSJ International Conference on Intelligent Robots and Systems (IROS)*, pages 4758–4765. IEEE, 2018.

- [21] Tixiao Shan, Brendan Englot, Drew Meyers, Wei Wang, Carlo Ratti, and Daniela Rus. Lio-sam: Tightly-coupled lidar inertial odometry via smoothing and mapping. In *2020 IEEE/RSJ international conference on intelligent robots and systems (IROS)*, pages 5135–5142. IEEE, 2020.
- [22] Tixiao Shan, Brendan Englot, Carlo Ratti, and Daniela Rus. Lvi-sam: Tightly-coupled lidar-visual-inertial odometry via smoothing and mapping. In *2021 IEEE international conference on robotics and automation (ICRA)*, pages 5692–5698. IEEE, 2021.
- [23] Shaoshuai Shi, Xiaogang Wang, and Hongsheng Li. Pointrcnn: 3d object proposal generation and detection from point cloud. In *Proceedings of the IEEE/CVF conference on computer vision and pattern recognition*, pages 770–779, 2019.
- [24] Xuebo Tian, Zhongyang Zhu, Junqiao Zhao, Gengxuan Tian, and Chen Ye. Dl-slot: Dynamic lidar slam and object tracking based on collaborative graph optimization. *arXiv preprint arXiv:2212.02077*, 2022.
- [25] Victor Vaquero, Kai Fischer, F. Moreno-Noguer, A. Sanfeliu, and Stefan Milz. Improving map re-localization with deep ‘movable’ objects segmentation on 3d lidar point clouds. *2019 IEEE Intelligent Transportation Systems Conference (ITSC)*, pages 942–949, 2019.
- [26] Chieh-Chih Wang, Charles Thorpe, Sebastian Thrun, Martial Hebert, and Hugh Durrant-Whyte. Simultaneous localization, mapping and moving object tracking. *The International Journal of Robotics Research*, 26(9):889–916, 2007.
- [27] Xinsuo Weng, Jianren Wang, David Held, and Kris Kitani. Ab3dmot: A baseline for 3d multi-object tracking and new evaluation metrics. *arXiv preprint arXiv:2008.08063*, 2020.
- [28] Hai Wu, Wenkai Han, Chenglu Wen, Xin Li, and Cheng Wang. 3d multi-object tracking in point clouds based on prediction confidence-guided data association. *IEEE Transactions on Intelligent Transportation Systems*, 23(6):5668–5677, 2021.
- [29] Hongru Xiao, Yanqun Han, Junqiao Zhao, Jiafeng Cui, Lu Xiong, and Zhuoping Yu. Lio-vehicle: A tightly-coupled vehicle dynamics extension of lidar inertial odometry. *IEEE Robotics and Automation Letters*, 7(1):446–453, 2021.
- [30] Wei Xu, Yixi Cai, Dongjiao He, Jiarong Lin, and Fu Zhang. Fast-lio2: Fast direct lidar-inertial odometry. *IEEE Transactions on Robotics*, 2022.
- [31] Wei Xu and Fu Zhang. Fast-lio: A fast, robust lidar-inertial odometry package by tightly-coupled iterated kalman filter. *IEEE Robotics and Automation Letters*, 6(2):3317–3324, 2021.
- [32] Sheng Yang, Xiaoling Zhu, Xing Nian, Lu Feng, Xiaozhi Qu, and Teng Ma. A robust pose graph approach for city scale lidar mapping. In *2018 IEEE/RSJ International Conference on Intelligent Robots and Systems (IROS)*, pages 1175–1182. IEEE, 2018.
- [33] Shichao Yang and Sebastian Scherer. Cubeslam: Monocular 3-d object slam. *IEEE Transactions on Robotics*, 35(4):925–938, 2019.
- [34] Haoyang Ye, Yuying Chen, and Ming Liu. Tightly coupled 3d lidar inertial odometry and mapping. In *2019 International Conference on Robotics and Automation (ICRA)*, pages 3144–3150. IEEE, 2019.
- [35] Ji Zhang and Sanjiv Singh. Loam: Lidar odometry and mapping in real-time. In *Proceedings of Robotics: Science and Systems Conference*, June 2014.
- [36] Jun Zhang, Mina Henein, Robert Mahony, and Viorela Ila. Vdo-slam: a visual dynamic object-aware slam system. *arXiv preprint arXiv:2005.11052*, 2020.
- [37] Shibo Zhao, Zheng Fang, HaoLai Li, and Sebastian Scherer. A robust laser-inertial odometry and mapping method for large-scale highway environments. In *2019 IEEE/RSJ International Conference on Intelligent Robots and Systems (IROS)*, pages 1285–1292. IEEE, 2019.